Chemical Engineering Journal 239 (2014) 274–283

Contents lists available at ScienceDirect

Chemical Engineering Journal

journal homepage: www.elsevier.com/locate/cej

Effects of temperature, pore dimensions and adsorbate on the transition from pore blocking to cavitation in an ink-bottle pore

Nikom Klomkliang [a,b], D.D. Do [a,*], D. Nicholson [a]

[a] School of Chemical Engineering, University of Queensland, St. Lucia QLD 4072, Australia
[b] Chemical Engineering, Faculty of Engineering, Naresuan University, Phitsanulok 65000, Thailand

HIGHLIGHTS

- Evolution of hysteresis loop with *temperature*, pore dimensions and adsorbate.
- Fused hysteresis loop of IUPAC and de Boer types.
- Double maxima in excess isotherms under supercritical conditions.

ARTICLE INFO

Article history:
Received 7 August 2013
Received in revised form 5 November 2013
Accepted 9 November 2013
Available online 19 November 2013

Keywords:
Adsorption
Ink-bottle pore
Pore blocking
Cavitation
Molecular simulation
Hysteresis

ABSTRACT

We have carried out comprehensive GCMC molecular simulations to study the effects of temperature (ranging from sub-critical to supercritical), cavity and neck dimensions, and adsorbate on the transition from pore blocking to cavitation in slit shaped ink-bottle pores. Varying these parameters affects, not only the position and the size of the hysteresis loop, but also its shape, which can change from H1, typical for pore blocking, to H1 or H2 combined with Type C (in the de Boer classification). The combined loops can either be fused loops or appear as two separate loops, one of which is of Type H1 and the other Type C. Another highlight of our simulation study is the double maxima in the adsorption isotherm at a supercritical temperature which results from the sigmoidal shape in the plot of bulk gas density versus pressure and the compression of the adsorbate in the confined space at high pressures.

© 2013 Elsevier B.V. All rights reserved.

1. Introduction

Hysteresis associated with capillary condensation and evaporation in porous materials has been the subject of immense interest for over 100 years [1], especially the search for the controlling mechanisms of adsorption and desorption. Adsorption in mesopores gives rise to hysteresis when the temperature is less than the critical hysteresis temperature and pore size is greater than a critical value [2,3].

Materials such as activated carbon, porous glass and silica gel consist of interconnected networks of pores of various shape and size, and their experimental isotherms can exhibit single or double steps in the hysteresis loop [2,4–18]. When hysteresis shows two distinct steps, the first, at lower pressure, is associated with condensation and evaporation in the smaller pores and the second with the same processes in wider pores. If the adsorbate–adsorbent system is wetting, adsorption proceeds by molecular layering, followed by condensation when both ends of a pore are exposed to the bulk surroundings, or by the advance of a meniscus from the closed end if one end of the pore is closed. Desorption, on the other hand, takes place by two processes which occur in conjunction: (1) the withdrawal of menisci from the pore mouth, and (2) the stretching of the condensed fluid in the interior region to a pressure where bubbles (cavities) appear in the adsorbate. When the first process dominates, the desorption mechanism is described as pore blocking, and as cavitation if stretching of the condensed fluid reaches the stability limit before the menisci have travelled to the pore interior. Both modes of evaporation can be illustrated by simulations using a simple ink-bottle pore model by tuning the neck size [19–23]. For a given adsorbate–adsorbent pair and temperature, the mechanism of desorption changes from pore-blocking to cavitation as the neck size decreases [20–24]. The cavitation pressure is a fluid property only when the cavity is large, typically greater than 7 nm for argon adsorption at 87 K, but is dependent on the cavity size for smaller cavities, because of the the overlap of adsorbent potential from closely spaced pore walls creates a stabilization effect [25,26]. The neck length can affect evaporation in an interesting way: Even when the neck size is

* Corresponding author.
E-mail address: d.d.do@uq.edu.au (D.D. Do).

1385-8947/$ - see front matter © 2013 Elsevier B.V. All rights reserved.
http://dx.doi.org/10.1016/j.cej.2013.11.019

smaller than the value at which cavitation normally occurs, evaporation can switch to pore blocking when the neck is very short; the shorter the neck, the greater the desorption pressure. While the cavity size affects the cavitation pressure for small cavities and the neck dimensions (width and length) affect the governing mechanism for desorption, temperature can also affect the desorption mechanism, which changes from pore blocking to cavitation at high temperature, because stretching of the condensed fluid in the cavity, overrides the process of meniscus withdrawal. This has been observed both experimentally and theoretically [4,7,11]. The change of evaporation mechanism for a given adsorbent, can also switch from pore blocking to cavitation as the pressure is reduced, and this change depends strongly on the pore structure and temperature [11,18,27]. Finally, the adsorbate molecule can also affect the desorption mechanism; for example Reichenbach and co-worker [11] observed pore blocking for argon adsorption in porous glass at 77 K, but found cavitation to be the mechanism for nitrogen at the same temperature.

Despite numerous simulation studies, there is still no systematic investigation into the effects of pore dimensions, temperature and adsorbate on the switch in the mechanism of desorption, from pore blocking to cavitation, in ink-bottle pores. It is the objective of this paper to fill this gap.

2. Theory

2.1. Fluid–fluid potential model

Argon was modelled as a single Lennard Jones (LJ) site and the 2CLJ + 3q N_2 (two LJ sites and three partial charges) model was chosen for nitrogen [28]. Their molecular parameters are listed in Table 1.

2.2. Fluid–solid potential model

A graphitic ink-bottle pore, with planar walls, connected to a gas reservoir via a neck is shown in Fig. 1. We used the Bojan-Steele equation [29–31] to calculate the fluid–solid potential energy with a 0.34 nm spacing between the two adjacent graphite layers, which are finite in the y-direction and infinite in the x-direction. The box length in the x-direction is 5 nm and periodic boundary conditions are applied at boundaries in this direction.

2.3. Grand canonical Monte Carlo (GCMC)

The standard Metropolis algorithm [32] was applied with equal probabilities of move rotation, insertion, and deletion. The cut-off radius was set at half of the box length and 1.2×10^8 configurations were run for both equilibration and sampling.

The average absolute and excess volumetric densities are defined by:

$$\rho_{\text{pore}}^{\text{ABS}} = \frac{\langle N \rangle}{V_{\text{acc}}}; \quad \rho_{\text{pore}}^{\text{EXC}} = \frac{\langle N \rangle - \rho_{\text{b}} V_{\text{acc}}}{V_{\text{acc}}} \tag{1}$$

where ρ_{b} is the bulk molecular density, $\langle N \rangle$ is the ensemble average of the number of particles in the pore, and V_{acc} is the accessible pore volume [33].

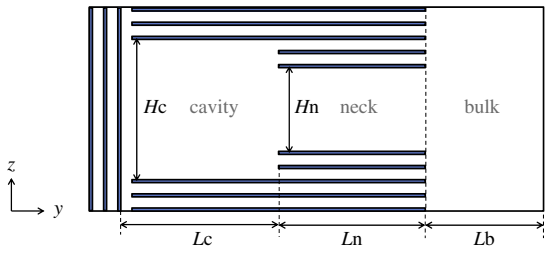

Fig. 1. Schematic diagrams of the ink-bottle pore with finite length in the y-direction and infinite length in the x-direction (perpendicular to the page). The length of bulk phase, Lb is fixed at 4 nm for all the systems studied.

The system was divided into meshes in the y- and z-directions to calculate the 2-dimensional (2D) density which is given by:

$$\rho(y,z) = \frac{\langle N_{(\Delta y, \Delta z)} \rangle}{L_x \Delta y \Delta z} \tag{2}$$

where N is the number of molecules in the mesh bounded by $(y-\Delta y/2,\ y+\Delta y/2)$ and $(z-\Delta z/2,\ z+\Delta z/2)$ and L_x is length in the x-direction. The mesh size was chosen to be $\Delta y = \Delta z = 0.1\sigma$.

3. Results and discussion

3.1. Ar adsorption at less than the critical hysteresis temperature

We first investigate argon adsorption in an ink-bottle pore whose cavity width is 3 nm and neck width is 2.3 nm. Note that in this small cavity and the force per unit area exerted by the cavitation pressure is less than the tensile strength of the bulk fluid because of the stabilization of the condensed fluid by the external field from the adsorbent. The lengths of the cavity and the neck were 10 nm. Fig. 2 shows the isotherms for temperatures from 60 K to 150 K. For ease of discussion, we define in Table 2 various terms that are used throughout the discussion.

3.1.1. Adsorption at 60 K

At this very low temperature, adsorption proceeds by molecular layering, followed by the formation of a meniscus at the bottom of the cavity because of the enhanced solid fluid interactions at the corners and the enhanced fluid–fluid interaction resulting from the shorter distances between neighbouring molecules at the curved interface (Fig. 3, top graph).

Once the meniscus is formed, the cavity behaves like a closed end pore while the neck behaves like an open end pore because of the gas-like fluid at its two ends. The meniscus then advances towards the junction as the pressure is increased (to Point A1) because at 60 K this process dominates the growth of molecular layers in the neck. When the meniscus has reached the junction (Point A2), the neck changes from an open end pore to a closed end pore (closed by the condensed fluid at the junction). Since the neck is smaller than the cavity, there is an advanced condensation in the neck (Point A3). The term "advanced" is because the condensation in the neck would occur at a higher pressure if its two ends were open to gas phase. The reason for this advanced condensation is because once the cavity is filled, any closed end pores whose sizes

Table 1
Molecular parameters for Ar and N_2.

Model	Site	x (nm)	y (nm)	z (nm)	σ (nm)	ε/k_{B} (K)	Charge (e)
Ar	Ar	0	0	0	0.3405	119.8	0
2CLJ + 3q N_2	N	0.055	0	0	0.331	36	−0.482
	N	−0.055	0	0	0.331	36	−0.482
	Centre	0	0	0	0	0	0.964

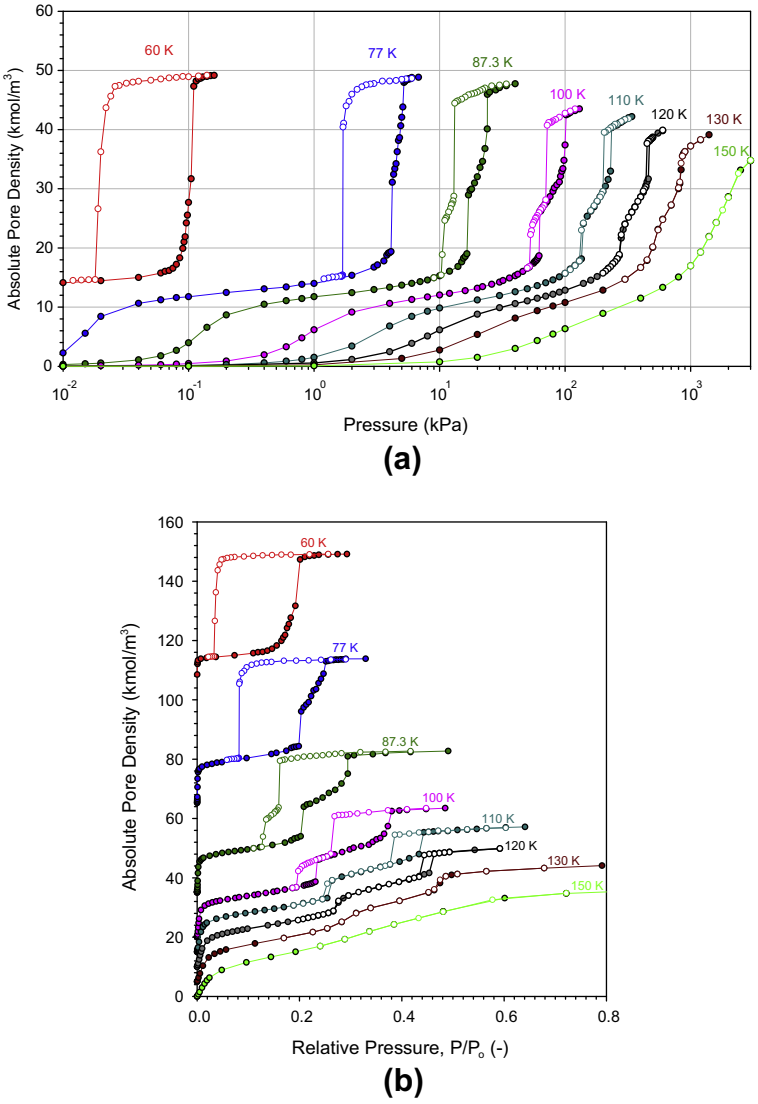

Fig. 2. Argon adsorbed in an ink-bottle pore having cavity width (*Hc*) 3 nm, cavity length (*Lc*) 10 nm, neck width (*Hn*) 2.3 nm, and neck length (*Ln*) 10 nm, at temperatures ranging from 60 to 150 K. Absolute pore density is plotted as a function of (a) pressure on a semi-log-scale and (b) relative pressure on a linear-scale.

Table 2
Definitions of terms used in this work.

Term	Definition
Open end pore	Finite pore with both ends open to adsorptive gas phase
Closed end pore	Finite pore with one end closed and the other end open to the gas phase
Closed pore	Finite pore with both ends closed by either a solid wall or liquid adsorbate of adjacent pores
The junction	The position at which the cavity and neck are joined together

are smaller than the cavity must have already been filled. This is illustrated in the middle and bottom graphs in Fig. 3 where we have plotted the densities contributed separately by the cavity and the neck. The sharp jump along the adsorption branch is due to the neck. This is not widely recognized in the literature of ink-bottle pore because condensation is always believed to be due to the cavity. For other conditions the condensation along the adsorption branch is due to the cavity as we will show later.

On desorption, pore blocking is the controlling mechanism for evaporation. A meniscus is formed at the pore mouth and recedes into the pore interior. At 60 K, this process stretches the condensed fluid, and therefore the meniscus, starting from the neck opening, travels towards the junction (Point A6) and when it reaches the junction the cavity changes from a closed pore to a closed-end pore. Since the adsorbate from the smaller closed end pore (which is the neck) has evaporated, any closed end pores that are larger in size must have already evaporated. This means that we have an instant evaporation of the cavity from Point A6 to Point A7, which is confirmed by the very sharp decrease in the adsorption density of the cavity (middle graph in Fig. 3). It must be stressed that this sharp evaporation is *not* cavitation, but rather a cavitation-like pore blocking, a phenomenon that is a consequence of the switch in the behaviour of the cavity from that of a closed pore to that of a closed end pore [23]. Interestingly, the shape of the hysteresis

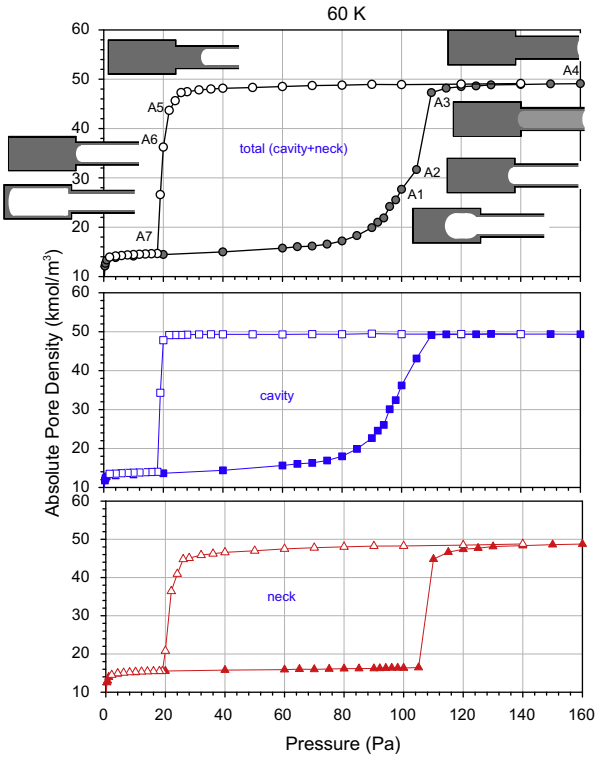

Fig. 3. Argon adsorption isotherms evaluated separately in the cavity, pore neck and in the whole pore (cavity and neck) at 60 K corresponding to Fig. 2.

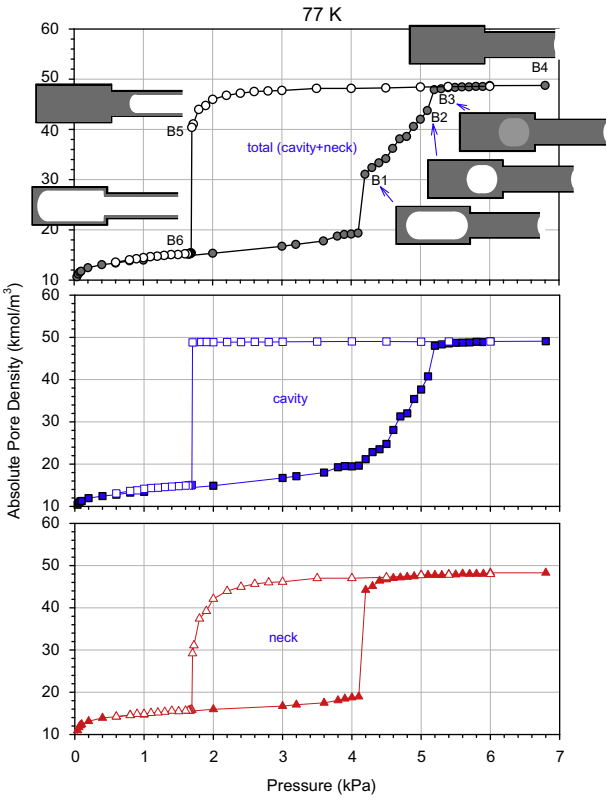

Fig. 4. Argon adsorption isotherms separately evaluated in the cavity, pore neck and whole pore (cavity and neck) at 77 K corresponding to those of Fig. 2.

loop for the ink-bottle pore is closer to Type H1, than to Type H2 as is usually attributed to ink-bottle pores [7]. This is due to the relative capacities between the cavity and the neck. When the neck is shorter in length, the density jump from A2 to A3 (due to the neck) is smaller, and therefore the hysteresis loop will change from Type H1 as seen in Fig. 3 to Type H2.

3.1.2. Adsorption at 77 K

When the temperature is increased to 77 K adsorption at low pressures occurs at the corners of the pore to form a meniscus at the closed end, as also happens at 60 K (Fig. 4). However, this temperature is high enough for the formation of multiple layers on the surfaces, and as a result condensation occurs in the neck (Point B1) before the meniscus can travel further away from the closed end. This is the first condensation, due to the neck, as seen in the overall isotherm as well as in the density of the neck. When the pressure is further increased the pore density is gradually increased due to the advance of the meniscus from the closed end, making the gas-like core (bubble) smaller with pressure. The bubble is located close to the junction at Point B2 (just before the condensation in the cavity)when there is condensation in the cavity (vertical line B2–B3). This is the second condensation in the isotherm.

The evaporation at this temperature is the same as that discussed earlier for 60 K, i.e. via cavitation-like pore blocking [23]. This is confirmed by the knee in the density plot for the neck and the constant density in the cavity just before evaporation (Point B5), followed by a sharp evaporation in the cavity to Point B6. The hysteresis loop at 77 K can be described as a combination of Type H2 and Type C since the individual loops associated with the cavity and neck are of Types H2 and C, respectively.

3.1.3. Adsorption at 87.3 K

The isotherm at 87.3 K is shown in the top plot in Fig. 5, and the densities of the cavity and the neck in the middle and bottom plots.

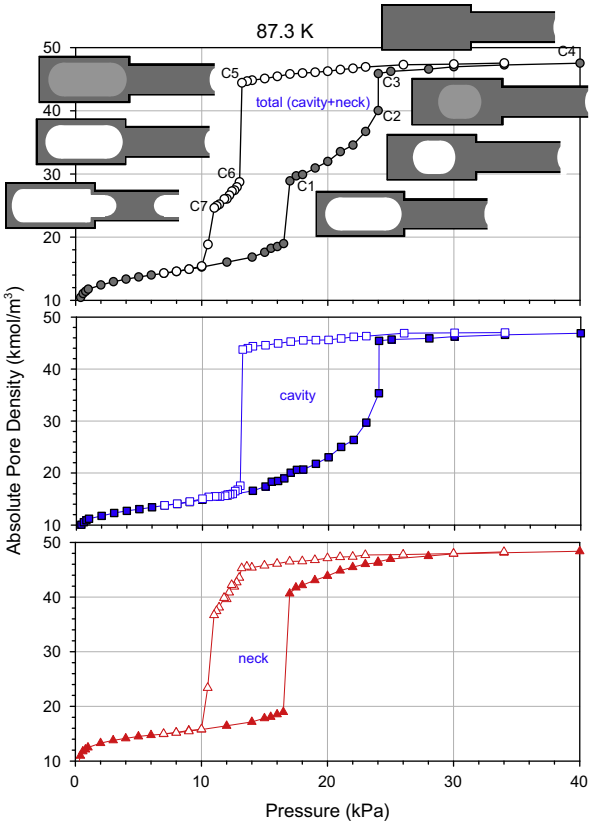

Fig. 5. Argon adsorption isotherms separately evaluated in the cavity, pore neck and whole pore (cavity and neck) at 87.3 K corresponding to that of Fig. 2.

The hysteresis loop is a combination of Type H1 and Type C since the individual loops, associated with the cavity and the neck, are of Types H1 and C, respectively. The capillary condensation occurs in two stages, corresponding to that in the neck and that in the cavity sequentially, as observed at 77 K. However, there is a subtle difference: at 87.3 K, the bubble is in the centre of the cavity but it remains close to the junction at 77 K, before it collapses at condensation, and furthermore the bubble size at 87.3 K is larger, prior to condensation.

On desorption, a meniscus is formed at the mouth of the neck and recedes only slightly as pressure is decreased from Point C4 to C5. At the same time, the condensed fluid in the cavity is stretched, as seen the 2D-density plot in Fig. 5, and since the stretching dominates the withdrawal of the meniscus, cavitation occurs at C5, and the density decreases sharply from C5 to C6, where the neck behaves like an open end pore, and on further reduction in pressure evaporation from the neck occurs at C7, followed by thinning of the adsorbed layers in the neck as well as in the cavity. Thus we see that the desorption mechanism for cavitation at 87.3 K is different from those at the lower temperatures, 60 and 77 K, where the evaporation is a cavitation-like pore blocking mechanism. It can be concluded that the stretching of a condensed fluid is more sensitive to temperature change than is the withdrawal of a meniscus; hence cavitation-like pore blocking switches to a cavitation mechanism for evaporation from the cavity as temperature is increased.

3.1.4. Adsorption at 100–120 K

The isotherm at 100 K is shown in Fig. 6. The mechanisms for adsorption and desorption are the same as those at 87.3 K, elaborated above.

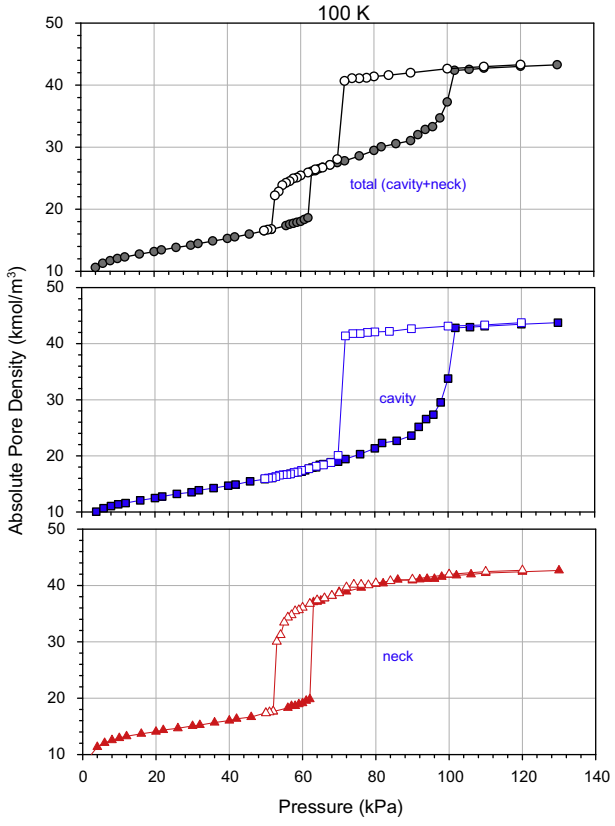

Fig. 6. Argon adsorption isotherms separately evaluated in the cavity, pore neck and whole pore (cavity and neck) at 100 K corresponding to that of Fig. 2.

The only difference is that the fused hysteresis loop is now broken into two distinct loops, the first being associated with the neck and the second with the cavity. As temperature is increased to 110 K and 120 K, the mechanisms remain the same, but the two loops become smaller until the first one, associated with the neck, disappears at 120 K. The second loop also disappears as temperature is increased further as we shall show in the next section.

3.1.5. Adsorption at 130 K and 150 K

These temperatures are above the critical hysteresis temperature and the isotherms are reversible as shown in Fig. 7. At 130 K, adsorption proceeds by filling the neck, followed by condensation in the cavity. At higher temperatures there is more fluctuation in the cavity than at lower temperatures, as seen in the snapshot plot for Point D3. It could be argued that at high temperatures adsorption is a process of compressing the adsorbate, and desorption is one of rarefaction, resulting in reversible isotherms.

An interesting point is that the 130 K isotherm, although reversible, shows a sharp change in density when the cavity is filled. This could be viewed as condensation in a poorly defined bubble as pressure is increased and cavitation of the condensed fluid when pressure is decreased. This implies that cavitation can occur in a reversible isotherm, i.e. independent of the appearance of a hysteresis loop, a feature which has not been recognized in the previous literature.

3.1.6. Temperature dependence of the condensation and evaporation pressures

The temperature dependence of the condensation and evaporation pressures is shown in Fig. 8a. We see that the condensation curve of the neck crosses the evaporation curve of the cavity at a dimensionless temperature, $\theta = (T-T_{tr})/(T_c-T_{tr})$, of about 0.17. When θ is greater than 0.17, the condensation and evaporation curves for the cavity are distinct from the corresponding curves for the neck, reflecting the existence of two distinct hysteresis loops. The first loop, associated with the neck, disappears at $\theta = 0.4$, which is the critical hysteresis temperature of the neck. Thus, when θ is greater than 0.4, there is a single hysteresis loop, associated with the cavity, which decreases in area with temperature and disappears at the critical hysteresis temperature of $\theta = 0.7$.

When θ is less than 0.17, there is a fused hysteresis loop, the first portion being due to the neck and the second to the cavity. When $\theta < -0.1$ (below the triple point), the evaporation of the neck is higher than that of the cavity, we observe a single hysteresis loop with the sharp jump in the adsorption branch associated with the neck.

3.2. Effects of cavity length

In Fig. 9 we show isotherms at various temperatures for pores with cavity lengths decreased from 10 nm to 3 nm and 1.5 nm, with the other dimensions remaining the same as in Fig. 2. When the cavity length is 3 nm, the evaporation mechanism switches from cavitation-like pore blocking to cavitation as temperature increases in the same way as observed earlier for the longer cavity. However, the transition shifts to a higher temperature; when the cavity is 10 nm long (see Fig. 2) the transition temperature is between 77 K and 87.3 K but occurs at 87.3 K when the cavity is 3 nm long (see Fig. 9a). When the cavity length is very short (1.5 nm), the desorption boundary of the hysteresis loop has two stages at 77 K and 87.3 K; the first is due to the long neck and the second to the cavity. The latter follows a pore blocking mechanism because one dimension (1.5 nm) of the cavity is smaller than the neck size (see Fig. 9b). However, cavitation-like pore blocking is the mechanism of evaporation for 100 K, with no appearance of the second step.

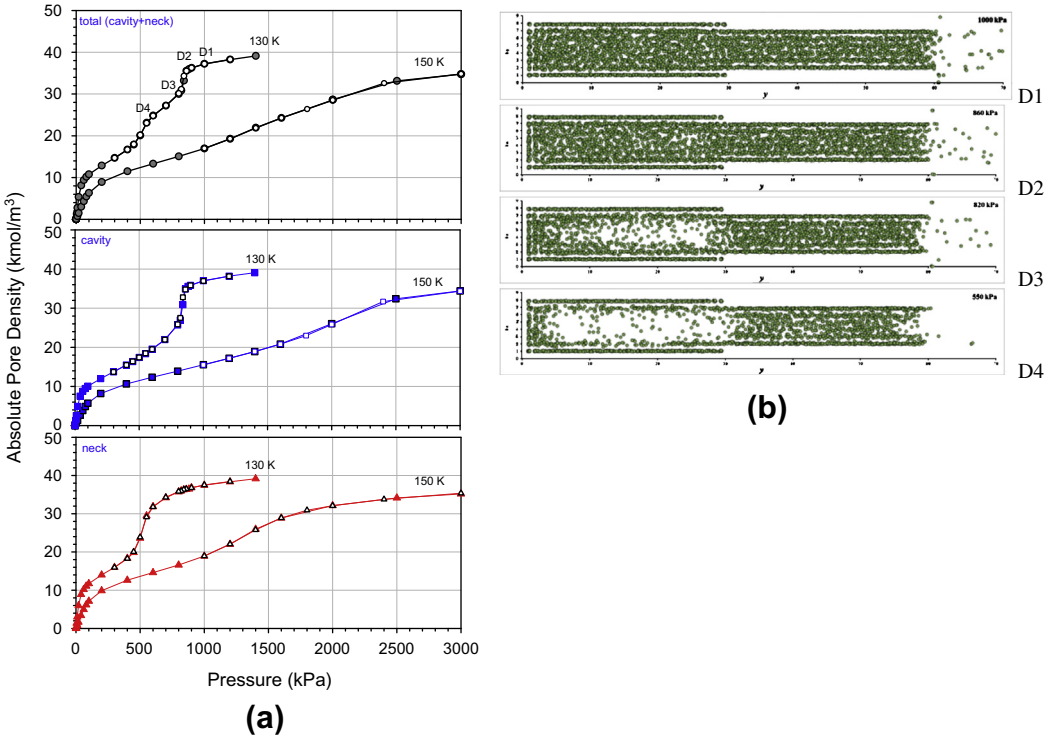

Fig. 7. (a) Argon adsorption isotherms separately evaluated in the cavity, pore neck and whole pore (cavity and neck) at 130 and 150 K corresponding to those in Fig. 2. (b) Snapshots along the desorption branch at 130 K where points D1 to D4 are the pressures marked in the top graph of Fig. 7a.

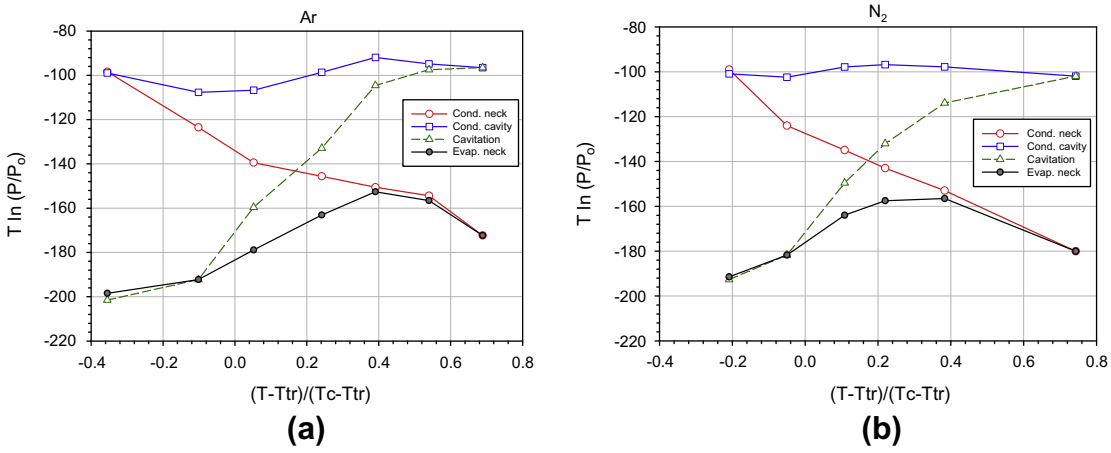

Fig. 8. Temperature dependence of condensation and evaporation pressures for adsorption in the bottle-pore (Hc = 3 nm, Lc = 10 nm, Hn = 2.3 nm, and Ln = 10 nm) for (a) argon and (b) nitrogen where T_{tr} is triple temperature and T_c is critical temperature.

3.3. Effects of cavity width when the neck width less than critical

Fig. 10 shows isotherms for the ink bottle-pore with larger cavity width, 5.7 nm, compared to 3 nm in the earlier model; the other dimensions are the same as those in Fig. 2.

Here the mechanism for evaporation at 60 K is cavitation-like pore blocking but changes to cavitation for temperatures greater or equal 77 K. The transition from pore blocking to cavitation occurs at a temperature lower than that in the 3 nm cavity (see Fig. 2) because the condensed fluid is stretched less readily in the smaller cavity where the holding potential is stronger, consequently the reduced cavitation pressure in the smaller cavity is 0.16, compared to 0.28 for larger cavities at 87.3 K as shown in Fig. 10b.

3.4. Ar adsorption in pores having neck width greater than critical

The temperature dependence of argon adsorption in the ink bottle-pore, having a cavity width of 4.3 nm and a neck width of 3.7 nm, greater than the critical value at 87.3 K, is examined in the temperature range from 87.3–120 K in Fig. 11.

At 87.3 K and 110 K, cavitation-like pore blocking is the mechanism for evaporation, and there is a single hysteresis loop of Type H1, in which the condensation along the adsorption branch is due

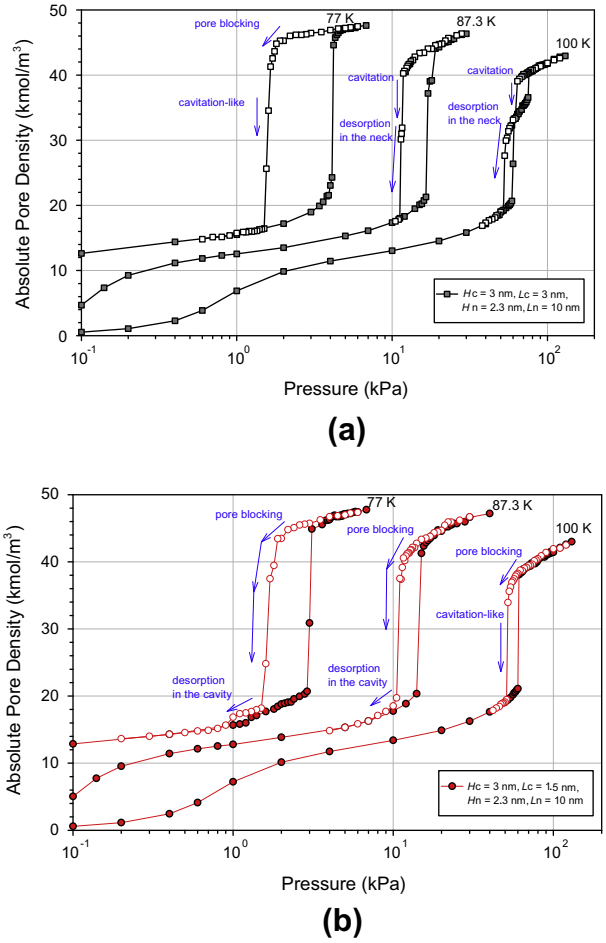

Fig. 9. Argon adsorbed in an ink bottle pore with shorter cavities at temperatures from 77 K to 100 K. Argon adsorbed in (a) 3 nm and (b) 1.5 nm lengths of the cavity.

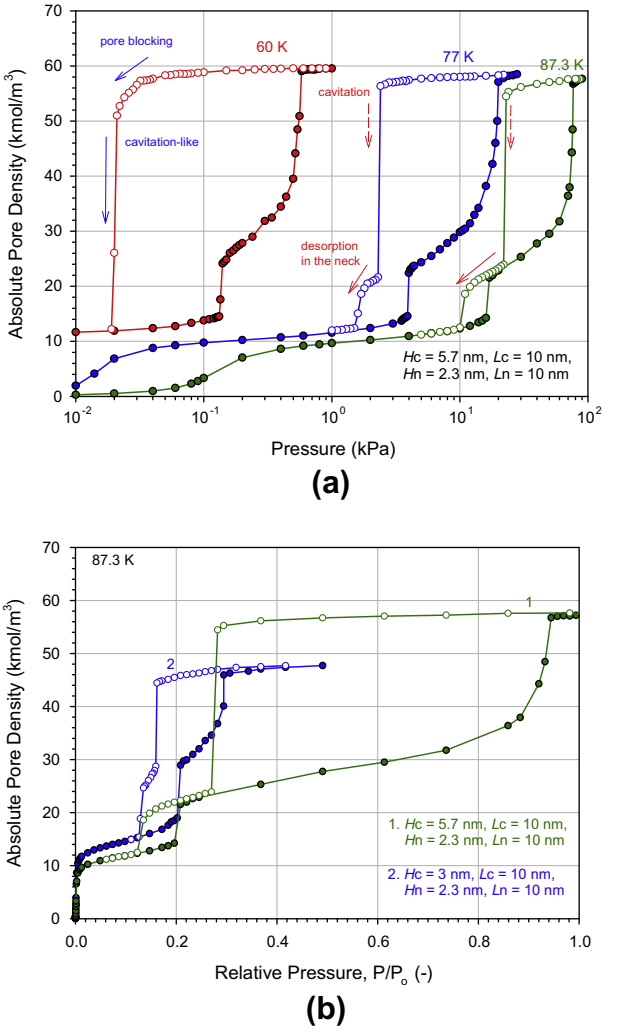

Fig. 10. (a) Argon adsorption isotherms at 60–100 K in ink bottle pores with a cavity width of 5.7 nm as a function of pressure on a semi-log-scale. (b) Argon adsorption in the pores with cavity widths of 5.7 and 3 nm at 87.3 K as a function of relative pressure on a linear-scale.

to the neck. These mechanisms are similar to those in the 3 nm wide cavity at 60 K. Cavitation-like pore blocking is also observed at 120 K, but the condensation occurs in two stages: in the neck followed by the cavity; this is similar to what was seen earlier for the ink-bottle pore with 3 nm wide cavity at 77 K. Therefore the transition temperature increases with an increase in the width of the pore neck.

3.5. Nitrogen adsorption

Nitrogen adsorption was also studied for the same ink-bottle pore as discussed in Section 3.1 (see Fig. 2); the isotherms at various temperatures are shown in Fig. 12.

The transition from pore blocking to cavitation is similar to that for argon; the only difference being that the transition temperature for nitrogen is between 60 K and 70 K while for argon it is between 77 K and 87.3 K.

Fig. 8b shows the temperature dependence of condensation and evaporation pressures for nitrogen adsorption and is similar to that for argon (i.e. sigmoid) seen in Fig. 8a.

3.6. Ar adsorption at subcritical temperatures at high pressures and supercritical temperatures

It has been observed [35,36] that, for argon adsorption in an open end slit pore under near-critical conditions, the excess pore

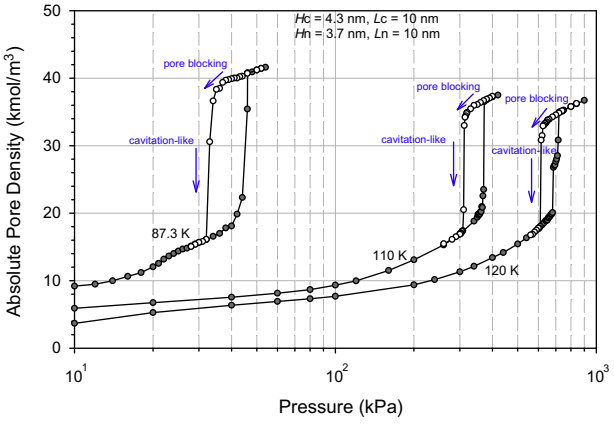

Fig. 11. Argon adsorption isotherms at 87.3–120 K in ink bottle pore having larger cavity sizes.

density exhibits a sharp maximum at the critical pressure (4.874 MPa) at temperatures close to the critical temperature (150.9 K). This is attributed to the sigmoidal behaviour of the bulk

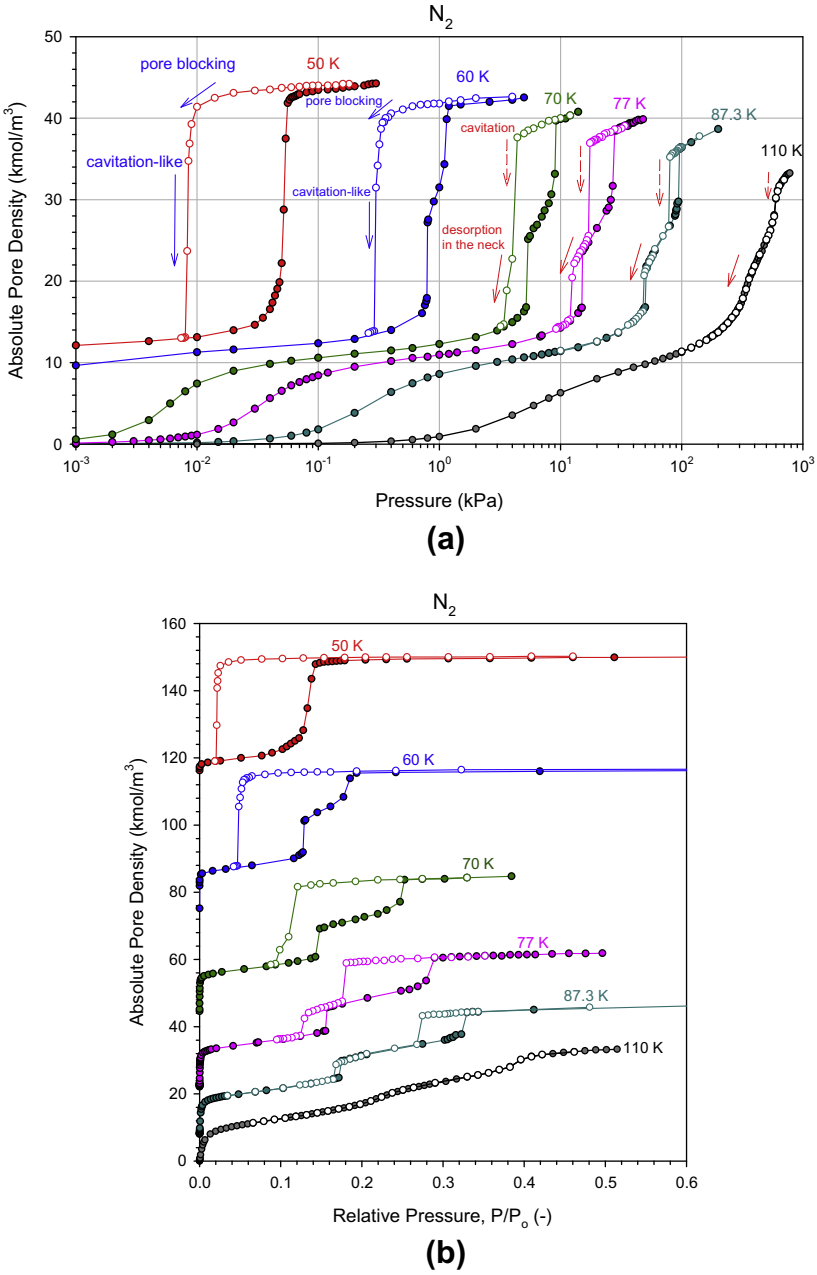

Fig. 12. Nitrogen adsorbed in an ink bottle-pore (Hc = 3 nm, Lc = 10 nm, Hn = 2.3 nm, and Ln = 10 nm) at temperatures ranging from 50–110 K. Absolute pore density is shown as a function of (a) pressure on a semi-log-scale and (b) relative pressure on a linear-scale. The reduced pressure is scaled against the simulation saturation vapour pressure [34].

density versus pressure (i.e. there is a significant change in density for a very small change in pressure). This type of maximum was also found at 130, 150 and 200 K for the ink-bottle pores studied here with the dimensions given in the caption to Fig. 13. To check the effects of the sigmoidal shape of the plot of bulk density (ρ_b) against pressure we also show, in Fig. 13, the first derivative of the bulk gas density with respect to pressure. It is seen that the derivative term ($d\rho_b/dP$) has a maximum at the pressure where the isotherm exhibits a sharp decrease.

At 200 K, the sigmoidal shape of the bulk density curve occurs at 10 MPa (Point E1) which is the position of first maximum in the isotherm; at this pressure the neck and cavity are filled with adsorbate. At higher pressures the adsorbate is further compressed as can be seen in the plot of the particle number against pressure (middle plot of Fig. 13), resulting in a second maximum at 400 MPa (Point E2), beyond which the increase in density in the bulk gas is greater than the increase in density in the pore. The second maximum does not appear in the isotherms at 130 K and 150 K because the pore is tightly packed with liquid condensate at pressures where the maximum in the excess isotherm occurs.

4. Conclusions

We have used grand canonical Monte Carlo simulation to investigate the transition from pore blocking to cavitation in the desorption branch of argon and nitrogen isotherms in carbonaceous ink-bottle pores. The transition temperature is found to increase with

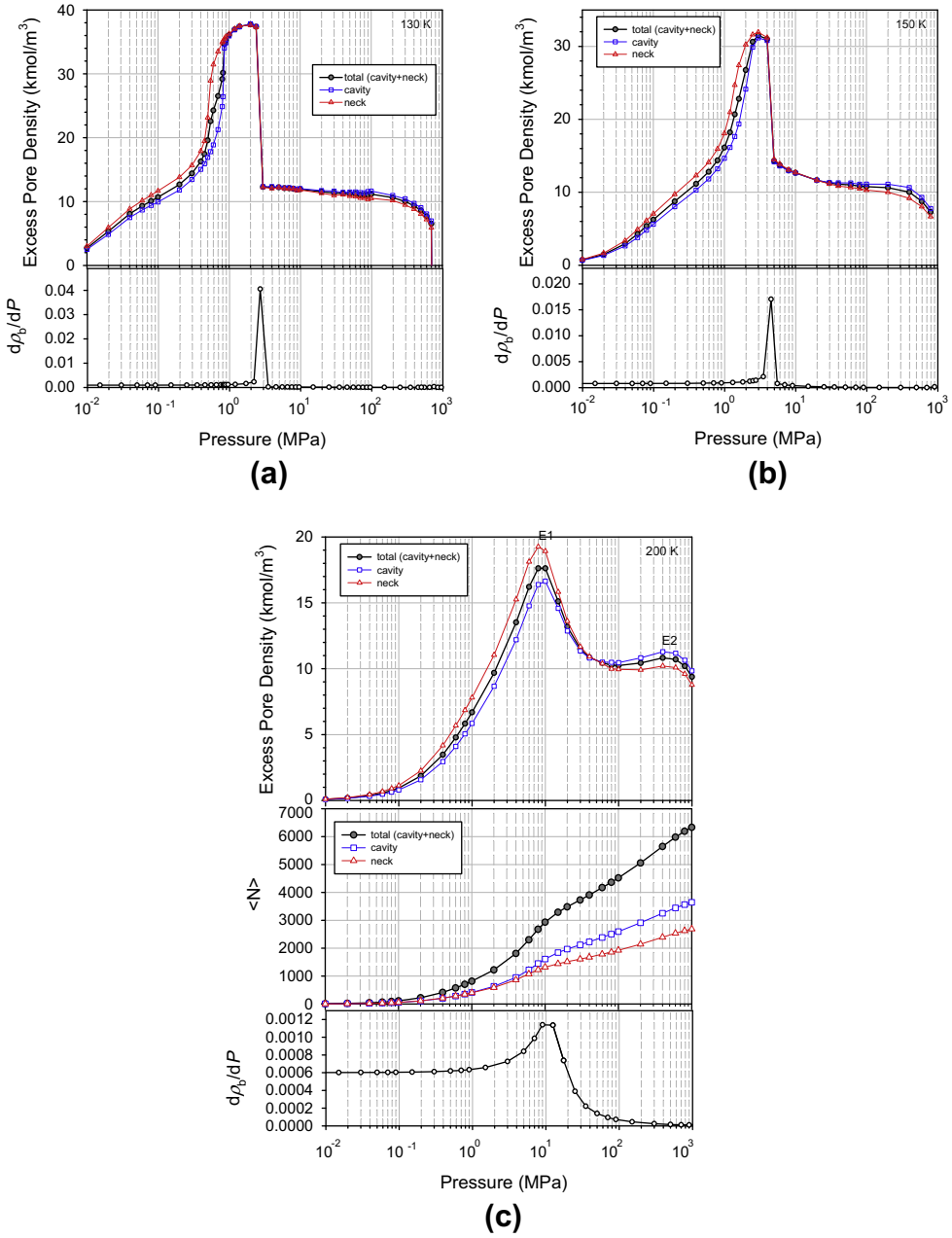

Fig. 13. Adsorption isotherms of argon in the bottle-pore (Hc = 3 nm, Lc = 10 nm, Hn = 2.3 nm, and Ln = 10 nm) at subcritical temperatures: (a) 130 K, (b) 150 K, and a supercritical temperature: (c) 200 K.

(i) increasing width of the pore neck, (ii) a decrease in neck length for very short necks (for longer necks, the transition temperature is insensitive to the length), (iii) a stronger holding potential for the adsorbate.

Argon adsorption in the ink-bottle-pore was also investigated at a supercritical temperature. There are two peaks in the plot of excess pore density versus pressure; the first peak is a consequence of the sigmoidal shape of the pressure dependence of the bulk gas density, and the second peak is due to the further compression of the adsorbate and is manifested only at high temperatures.

Acknowledgement

This project was supported by the Australian Research Council.

References

[1] T. Horikawa, D.D. Do, D. Nicholson, Capillary condensation of adsorbates in porous materials, Advances in Colloid and Interface Science 169 (2011) 40–58.
[2] K. Morishige, N. Tateishi, Adsorption hysteresis in ink-bottle pore, Journal of Chemical Physics 119 (2003) 2301–2306.
[3] K. Morishige, Adsorption hysteresis in ordered mesoporous silicas, Adsorption-Journal of the International Adsorption Society 14 (2008) 157–163.
[4] P.I. Ravikovitch, A.V. Neimark, Experimental confirmation of different mechanisms of evaporation from ink-bottle type pores: equilibrium, pore blocking, and cavitation, Langmuir 18 (2002) 9830–9837.
[5] M. Kruk, M. Jaroniec, Argon adsorption at 77 K as a useful tool for the elucidation of pore connectivity in ordered materials with large cagelike mesopores, Chemistry of Materials 15 (2003) 2942–2949.
[6] S.P. Rigby, R.S. Fletcher, Experimental evidence for pore blocking as the mechanism for nitrogen sorption hysteresis in a mesoporous material, The Journal of Physical Chemistry B 108 (2004) 4690–4695.
[7] K. Morishige, M. Tateishi, F. Hirose, K. Aramaki, Change in desorption mechanism from pore blocking to cavitation with temperature for nitrogen in ordered silica with cagelike pores, Langmuir 22 (2006) 9220–9224.

[8] A. Grosman, C. Ortega, Capillary condensation in porous materials. Hysteresis and interaction mechanism without pore blocking/percolation process, Langmuir 24 (2008) 3977–3986.
[9] K. Morishige, K. Yoshida, Neck size of ordered cage-type mesoporous silica FDU-12 and origin of gradual desorption, The Journal of Physical Chemistry C 114 (2010) 7095–7101.
[10] K. Morishige, T. Yasuki, Large-pore cagelike silica with necks of molecular dimensions, The Journal of Physical Chemistry C 114 (2010) 10910–10916.
[11] C. Reichenbach, G. Kalies, D. Enke, D. Klank, Cavitation and pore blocking in nanoporous glasses, Langmuir 27 (2011) 10699–10704.
[12] A.H. Lu, F. Schüth, Nanocasting pathways to create ordered mesoporous solids, Comptes Rendus Chimie 8 (2005) 609–620.
[13] C.J. Rasmussen, A. Vishnyakov, M. Thommes, B.M. Smarsly, F. Kleitz, A.V. Neimark, Cavitation in metastable liquid nitrogen confined to nanoscale pores, Langmuir 26 (2010) 10147–10157.
[14] K. Morishige, M. Ito, Capillary condensation of nitrogen in MCM-41 and SBA-15, Journal of Chemical Physics 117 (2002) 8036–8041.
[15] K. Morishige, N. Tateishi, S. Fukuma, Capillary condensation of nitrogen in MCM-48 and SBA-16, The Journal of Physical Chemistry B 107 (2003) 5177–5181.
[16] J. Liu, L. Zhang, Q. Yang, C. Li, Structural control of mesoporous silicas with large nanopores in a mild buffer solution, Microporous and Mesoporous Materials 116 (2008) 330–338.
[17] D.R. Sahu, L.Y. Hong, S.C. Wang, J.L. Huang, Synthesis, analysis and characterization of ordered mesoporous TiO2/SBA-15 matrix: effect of calcination temperature, Microporous and Mesoporous Materials 117 (2009) 640–649.
[18] A. Grosman, C. Ortega, Cavitation in metastable fluids confined to linear mesopores, Langmuir 27 (2011) 2364–2374.
[19] A. Vishnyakov, A.V. Neimark, Monte Carlo simulation test of pore blocking effects, Langmuir 19 (2003) 3240–3247.
[20] B. Libby, P.A. Monson, Adsorption/desorption hysteresis in ink bottle pores: a density functional theory and Monte Carlo simulation study, Langmuir 20 (2004) 4289–4294.
[21] C.Y. Fan, D.D. Do, D. Nicholson, On the cavitation and pore blocking in slit-shaped ink-bottle pores, Langmuir 27 (2011) 3511–3526.
[22] P.T.M. Nguyen, D.D. Do, D. Nicholson, On the cavitation and pore blocking in cylindrical pores with simple connectivity, The Journal of Physical Chemistry B 115 (2011) 12160–12172.
[23] P.T.M. Nguyen, C. Fan, D.D. Do, D. Nicholson, On the cavitation-like pore blocking in ink-bottle pore: evolution of hysteresis loop with neck size, The Journal of Physical Chemistry C 117 (2013) 5475–5484.
[24] L. Sarkisov, P.A. Monson, Modeling of adsorption and desorption in pores of simple geometry using molecular dynamics, Langmuir 17 (2001) 7600–7604.
[25] M. Thommes, B. Smarsly, M. Groenewolt, P.I. Ravikovitch, A.V. Niemark, Adsorption hysteresis of nitrogen and argon in pore networks and characterization of novel micro- and mesoporous silicas, Langmuir 22 (2006) 756–764.
[26] T.-W. Kim, R. Ryoo, M. Kruk, K.P. Gierszal, M. Jaroniec, S. Kamiya, O. Terasaki, Tailoring the pore structure of SBA-16 silica molecular sieve through the use of copolymer blends and control of synthesis temperature and time, The Journal of Physical Chemistry B 108 (2004) 11480–11489.
[27] P.T.M. Nguyen, D.D. Do, D. Nicholson, Pore connectivity and hysteresis in gas adsorption: a simple three-pore model, Colloids and Surfaces A: Physicochemical and Engineering Aspects 437 (2013) 56–58.
[28] J.J. Potoff, J.I. Siepmann, Vapor–liquid equilibria of mixtures containing alkanes, carbon dioxide, and nitrogen, AIChE Journal 47 (2001) 1676–1682.
[29] M.J. Bojan, W.A. Steele, Computer simulation of physisorption on a heterogeneous surface, Surface Science 199 (1988) L395–L402.
[30] M.J. Bojan, W.A. Steele, Computer-simulation of physisorbed Kr on a heterogeneous surface, Langmuir 5 (1989) 625–633.
[31] M.J. Bojan, W.A. Steele, Computer-simulation of physical adsorption on stepped surfaces, Langmuir 9 (1993) 2569–2575.
[32] M.P. Allen, T.P. Tildesley, Computer Simulation of Liquids, Clarendon, Oxford, 1987.
[33] D.D. Do, L.F. Herrera, H.D. Do, A new method to determine pore size and its volume distribution of porous solids having known atomistic configuration, Journal of Colloid and Interface Science 328 (2008) 110–119.
[34] C. Fan, D.D. Do, D. Nicholson, A new and effective Bin–Monte Carlo scheme to study vapour–liquid equilibria and vapour–solid equilibria, Fluid Phase Equilibria 325 (2012) 53–65.
[35] J. Specovius, G.H. Findenegg, Physical adsorption of gases at high pressures: argon and methane onto graphitized carbon black, Berichte Bunsen Physics Chemistry 82 (1978) 174–180.
[36] D.D. Do, H.D. Do, Adsorption of argon from sub- to supercritical conditions on graphitized thermal carbon black and in graphitic slit pores: a grand canonical Monte Carlo simulation study, Journal of Chemical Physics 123 (2005) 084701–84715.